

Atlantic Water Circulation and Properties Northwest of Svalbard During Anomalous Southerly Winds

Zoé Koenig^{1,2}, Amelie Meyer^{3,4}, Christine Provost⁵, Nathalie Sennéchaël⁵, Arild Sundfjord¹, and Jean-Claude Gascard⁵

¹Norwegian Polar Institute, Fram Centre, Tromsø, Norway, ²Geophysical Institute and Bjerknes Center for Climate Research, The University of Bergen, Bergen, Norway, ³Institute for Marine and Antarctic Studies, University of Tasmania, Hobart, TAS, Australia, ⁴Australian Research Council Centre of Excellence for Climate Extremes, University of Tasmania, Hobart, TAS, Australia, ⁵Laboratoire LOCEAN IPSL, Sorbonne Universites (UPMC, University Paris 6), CNRS, IRD, MNHN, Paris, France

Key Points:

- A SeaExplorer glider documented the Atlantic Water (AW) inflow west and north of Svalbard during a summer dominated by southerly winds
- Shelf-water lenses cooled and freshened the core of the AW inflow from below
- The AW “Svalbard Branch” above the Yermak Plateau was weak, which can be explained by the wind forcing

Correspondence to:

Z. Koenig,
zoe.koenig@uib.no

Citation:

Koenig, Z., Meyer, A., Provost, C., Sennéchaël, N., Sundfjord, A., & Gascard, J.-C. (2022). Atlantic Water circulation and properties northwest of Svalbard during anomalous southerly winds. *Journal of Geophysical Research: Oceans*, 127, e2021JC018357. <https://doi.org/10.1029/2021JC018357>

Received 17 DEC 2021

Accepted 5 JUN 2022

Abstract Atlantic Water (AW), the main source of heat and salt for the Arctic Ocean, undergoes large transformations (cooling and freshening) north of Svalbard as it flows near the surface above the Yermak Plateau (YP). In September 2017, a SeaExplorer ocean glider deployed in the West Spitsbergen Current (WSC) and recovered north of Svalbard documented the circulation and properties of the AW crossing the YP. The glider sampled the different branches of the AW flowing into the Arctic around the YP: the WSC, the Svalbard Branch (SB), the Yermak Pass Branch, and the Yermak Branch. Unusual southerly winds prevailed in summer 2017 impacting AW circulation in the region. Cold and fresh lenses of shelf-origin waters detached from the slope in the WSC to reach their density level below the core of the AW. This resulted in cooling and freshening of the AW inflow from below. The eastward current associated with the SB was found to be weak at its usual location above the 400 m isobath, likely the result of the adjustment of the flow influenced by anomalous southerly wind conditions.

Plain Language Summary The warm and salty Atlantic Water (AW) is the main source of heat and salt for the Arctic Ocean. This water mass enters the Arctic Ocean through the Barents Sea and the Fram Strait. The circulation pathways and the cooling and freshening that this water undergoes influence the variability of the Arctic sea ice and the marine ecosystems. In September 2017, an autonomous ocean glider deployed west of Svalbard and recovered north of Svalbard documented the circulation and properties of the different branches of the AW in this region at a time of anomalous southerly winds. Numerous cold and fresh lenses of shelf waters were found on the slope, detaching from the bottom and stabilizing just below the AW layer; they cool and freshen the AW flowing into the Arctic Ocean from below. The current associated with the AW inflow along the slope north of Svalbard in September 2017 was weak.

1. Introduction

Warm and salty Atlantic Water (AW) enters the Arctic Ocean via the Fram Strait and the Barents Sea, and colder and fresher Arctic Water exits the Arctic Ocean over the eastern continental slope of Greenland through the East Greenland Current and Canadian Archipelago (Tsubouchi et al., 2018). While the AW circulates around the Arctic, temperatures drop down by $3.74 \pm 0.76^\circ\text{C}$ and salinities by 0.62 ± 0.23 psu (Tsubouchi et al., 2018).

Some of the key locations for water mass transformation of the AW are west and north of Svalbard and in the Barents Sea where AW is in direct contact with the atmosphere. In the Barents Sea, AW cools significantly before entering the Arctic Ocean through the St. Anna Trough (Skagseth et al., 2020). In the West Spitsbergen Current (WSC), the AW cools by $\sim 0.2^\circ\text{C}$ per 100 km (Kolås & Fer, 2018). The WSC splits into different branches as the isobaths diverge when reaching the Yermak Plateau (YP). About 50% of the WSC recirculates directly in the Fram Strait (Hattermann et al., 2016; von Appen et al., 2016), while the other half enters the Arctic Ocean through three branches: the Yermak Branch (YB), the Svalbard Branch (SB) (Cokelet et al., 2008), and the Yermak Pass Branch (YPB) (Crews et al., 2018; Gascard et al., 1995; Koenig, Provost, Sennechaël, et al., 2017; Menze et al., 2019).

In the past decade, both the Barents Sea and the area north of Svalbard have witnessed major changes, including large losses of sea ice, likely playing a role in the observed Atlantification of the Eurasian Basin (Asbjørnsen

© 2022 The Authors.

This is an open access article under the terms of the [Creative Commons Attribution-NonCommercial License](https://creativecommons.org/licenses/by-nc/4.0/), which permits use, distribution and reproduction in any medium, provided the original work is properly cited and is not used for commercial purposes.

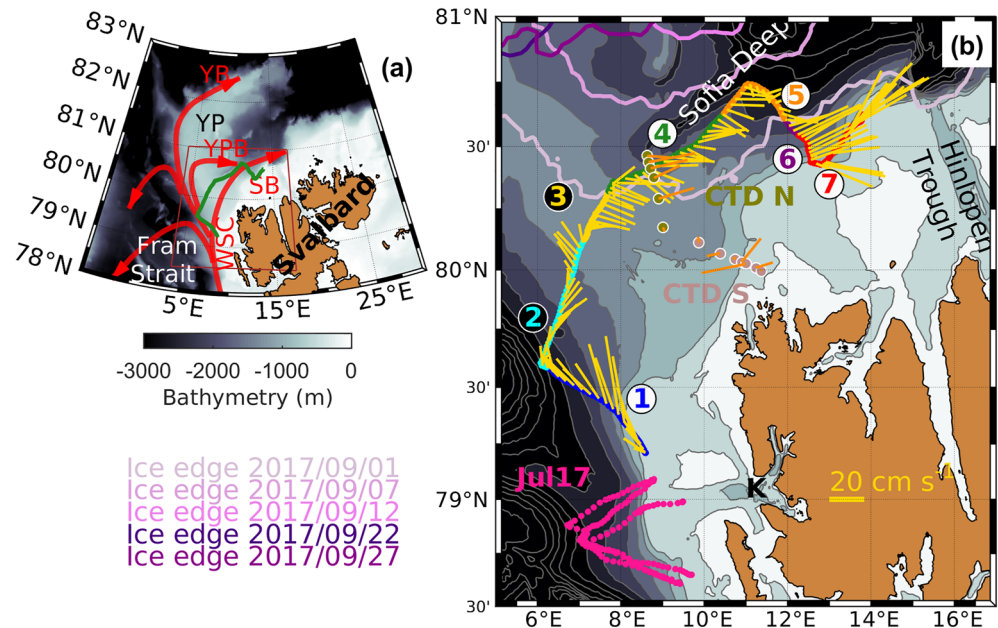


Figure 1. (a) Path around the Yermak Plateau. YB: Yermak Branch. YPB: Yermak Pass Branch. SB: Svalbard Branch. WSC: West Spitsbergen Current. The glider trajectory is indicated in green. (b) In detail trajectory of the glider with blue color at the beginning of the trajectory and red when the glider is picked up. Background is bathymetry from IBCAO-v3 (Jakobsson et al., 2012). Contours are bathymetry isolines every 200 m. The pink trajectory is the one of the SeaExplorer gliders deployed in July 2017 (see Koenig et al. (2018) for more details). The yellow arrows are the depth-averaged current intensities deduced from the dead-reckoning data from the glider and the orange arrows are the depth-averaged current intensities from the Lowered Acoustic Doppler Current Profiler for the ship stations. The pink/purple lines correspond to the ice edge (15% ice concentration), respectively, on 1, 7, 12, 22, and 27 September. Numbers in circles indicate the different zones that are used in the following figures. K:Kongsfjorden.

et al., 2020; Polyakov et al., 2017; Årthun et al., 2012). The reduced stratification characterizing the Atlantification preconditions deep winter convection over the Eurasian continental slope and favors large areas of open ocean without sea ice along the path of the AW above the slope (Athanasé et al., 2020; Ivanov et al., 2016; Koenig, Provost, Villaceros-Robineau et al., 2017). The reduced sea ice cover over the continental slope north of Svalbard can be seen as a precursor of what will happen in the Eurasian Basin.

Circulation patterns in the area north of Svalbard are affected by local wind forcing. Nilsen et al. (2021) demonstrate a significant correlation between the wind stress curl over the northeastern Fram Strait and volume transport anomaly across the YP. They also suggest that more frequent winter cyclones will increase the volume transport variability and pulses of warm water to the shelf areas north of Svalbard, which will impact ecosystems in the region.

In July and September 2017, we deployed a glider west and north of Svalbard to investigate the AW properties and pathways in this region (Figure 1). The July–August 2017 mission focused on the WSC (Koenig et al., 2018) and sampled cold and fresh lenses originating from the shelf and participating in the cooling and freshening of the core of the WSC. The presence of these lenses from the shelf can be related to the wind regime. Strong southerly winds cause upwelling of the warm AW onto the shelf in winter. Weak and/or northerly winds allow the modified AW formed by mixing with cold waters on the shelf to cascade down the slope, leading to lenses of colder and fresher water protruding into the WSC.

In September 2017, the glider documented the properties of the different AW branches around the YP north of Svalbard, which is the focus of this study.

2. Data and Methods

2.1. Mission Overview

The glider was deployed on 15 September 2017, 01:40 UTC west of Svalbard, in the WSC (79.2°N, 8.6°E, Figure 1) (Koenig, Beguery, et al., 2017). The glider followed the WSC before crossing the YP toward the Sofia Deep. The glider was recovered on the slope north of Svalbard on 23 September 2017, 16:30 UTC at 80.62°N, 13.83°E. The glider always operated in ice-free waters. At its northernmost location (80.7°N, 11.1°E), the glider was close to the sea ice edge (Figure 1) and had difficulties to reach the surface due to the presence of light surface lenses of very fresh water (see the following sections for more details).

The glider had been previously deployed in July–August 2017 (pink trajectory in Figure 1, Koenig et al. (2017)). During that earlier mission, it crisscrossed the WSC 6 times near the mouth of Kongsfjorden.

2.2. Glider Data Processing

The glider is a SeaExplorer glider from Alseamar (www.alseamar-alcen.com) equipped with a Glider Payload Conductivity Temperature Depth (GPCTD) from SeaBird, a dissolved oxygen sensor (Sea Bird SBE43F), and an optical sensor (EcoPuck from Wetlab) measuring Chlorophyll a (470/695 nm), colored dissolved organic matter (CDOM, 370/460 nm), and the total particle concentration or backscatter (backscattering at 700 nm). The glider sampled the ocean along a sawtooth trajectory from the surface down to a maximum depth of 700 m or near the bottom if shallower than 700 m, with an average horizontal distance of 1.7 km between each surfacing location. As the isopycnal slopes are much smaller than the pitch angle of the glider, each up and down dive can be considered as representing a vertical profile.

We use hereafter the International Thermodynamic Equations of Seawater (TEOS-10) framework (McDougall & Barker, 2011) with Conservative Temperature Θ (°C) and Absolute Salinity S_A (g kg⁻¹). Glider data were processed using the SOCIB toolbox (<https://github.com/socib/glidertoolbox>). Thermal lag issues of the GPCTD probe were corrected by applying the method of Garau et al. (2011). Although thermal lag corrections were applied, the thermocline and halocline gradients were so large that some differences remained between the up and down profiles in these layers in the salinity and related parameters (dissolved oxygen and chlorophyll a). The density was then despiked and interpolated, and salinity was recalculated from the temperature and the corrected density. For some profiles, the salinity measurements did not pass the quality control, which is why there is no salinity. Several reasons are possible, one of them being that at some point the glider encountered a very fresh and cold layer and some frazil ice could have then ended up in the conductivity cell.

Data were averaged on a 1-m vertical grid. Data from the glider were compared to the closest ship Conductivity Temperature Depth (CTD) data (in time and in space) collected during the accompanying research cruise (A-TWAIN 2017). A comparison between glider and ship CTD data resulted in an estimated glider accuracy of $\Delta\Theta \sim 0.005^\circ\text{C}$ and $\Delta S_A \sim 0.01 \text{ g kg}^{-1}$ (not shown). CDOM and total particle concentration are presented with the manufacturer sensor calibration and are, respectively, given in parts per billion (ppb) and per meter per steradian (m⁻¹ sr⁻¹). We use the Apparent Oxygen Utilization (AOU), defined as $\text{AOU} = [O_2]_s - [O_2]$, where $[O_2]_s$ is the solubility of the dissolved oxygen at the temperature and salinity of the media, and $[O_2]$ is the measured oxygen concentration by the glider.

Depth-averaged currents over each glider dive were computed from the dead-reckoning navigation of the glider and GPS fixes at the surface. The depth-averaged currents have been detided using the Arc5km2018 barotropic tidal model (Erofeeva & Egbert, 2020), a barotropic inverse tidal model on a 5-km grid that estimates the tidal currents using the main 8 constituents (M_2 , S_2 , N_2 , K_2 , K_1 , O_1 , P_1 , and Q_1) and 4 nonlinear components (M_4 , MS_4 , MN_2 , and $2N_2$). Maximum tidal amplitude was found on the YP as high as 0.23 m s⁻¹ (not shown).

2.3. Data From a Research Vessel

Complementary hydrographic data were collected during the A-TWAIN 2017 research cruise onboard R/V Lance (14 September to 26 September 2017). 13 CTD stations were performed on 24 September 2017 along a section above the southern YP, the southern part of the section (pale pink dots in Figure 1b) heading northwest and the northern parts (olive dots in Figure 1b) heading north and joining the glider trajectory. The ship-board CTD was

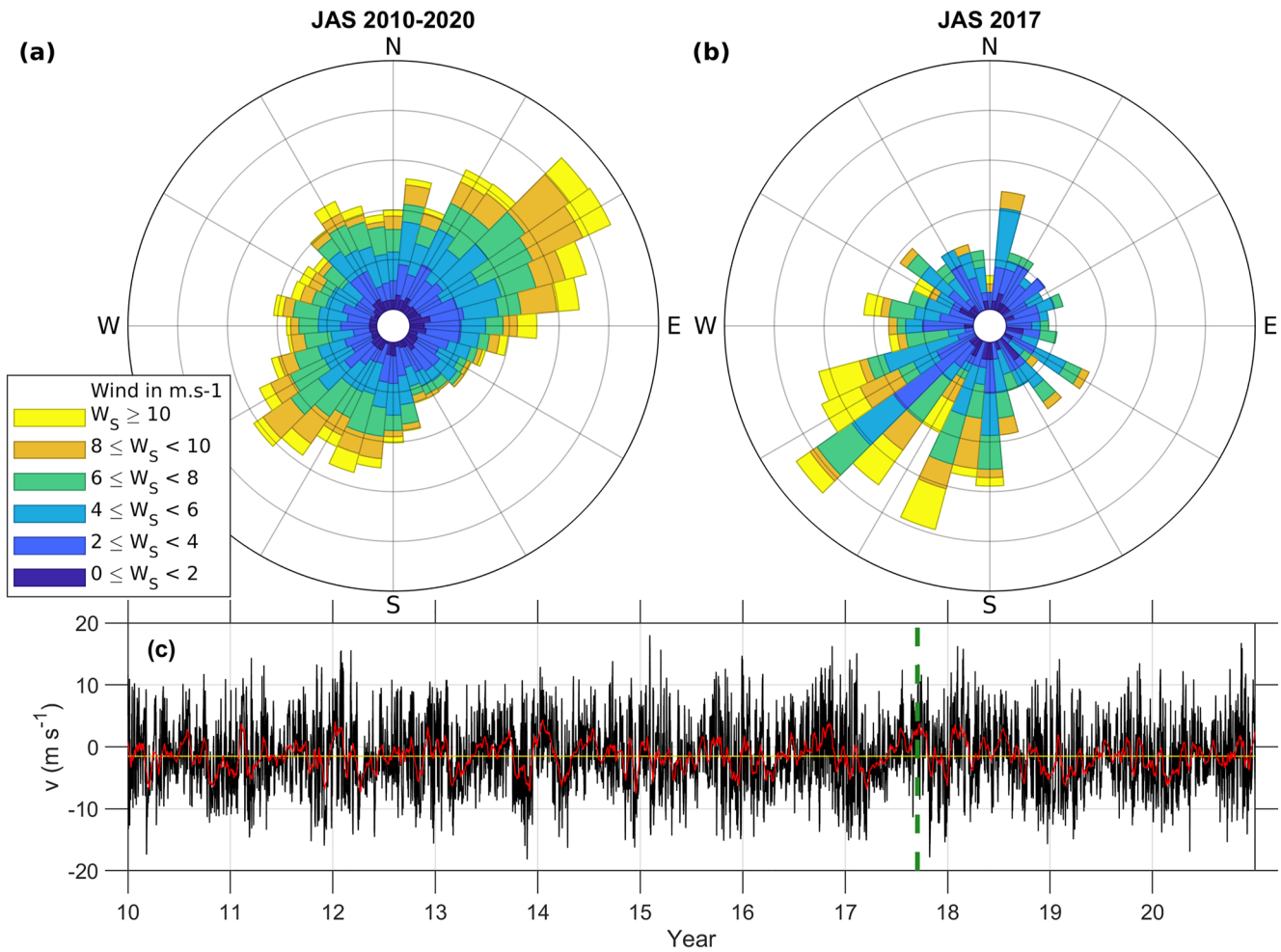


Figure 2. Wind rose diagrams of the wind speed (W_s) and direction north of Svalbard averaged over the box $80\text{--}80.7^\circ\text{N}$ and $8\text{--}14^\circ\text{E}$. (a) Over July–August–September 2010–2020. (b) Over July–August–September 2017. (c) Meridional component of the wind at 10 m averaged in the same box over 2010–2020. The red line is a 20 days running mean. The yellow line is the meridional wind averaged over 2010–2020. The green dashed line indicates the glider mission in September 2017.

a Sea-Bird Electronics SBE911+. Pressure, temperature, and practical salinity data are accurate to ± 0.5 dbar, $\pm 2 \times 10^{-3}^\circ\text{C}$, and $\pm 3 \times 10^{-3}$, respectively.

One 300 kHz RDI Workhorse (Teledyne RD Instrument (RDI) downward oriented) Lowered Acoustic Doppler Current Profiler (LADCP) was attached to the CTD frame to measure the zonal and meridional components of the velocity through the water column at each station with a 8-m vertical bin-size resolution. The LADCP data were processed onboard and postprocessed after the cruise using the LDEO Software developed by Thurnherr (2011). Estimates of the magnetic declination for each station based on date, latitude, and longitude using the NOAA magnetic field calculator (<https://www.ngdc.noaa.gov/geomag/calculators/magcalc.shtml>) were applied.

2.4. Environmental Data

10-m wind data were extracted from an ERA5 reanalysis set with a 6-hr resolution (Figure 2) from 2010 to 2020 (average over $79.5\text{--}80.5^\circ\text{N}$ and $8\text{--}14^\circ\text{E}$) (Hersbach et al., 2018). The southerly winds observed in summer 2017 deviate from the average for the past decade north of Svalbard where winds are predominantly northeasterlies (Figures 2a and 2b). Indeed, over the period 2010–2020, southerly winds larger than 8 m s^{-1} are found less than 5% of the time (Figure 2).

To look in more detail into the wind forcing in September 2017, we extracted the 10 m wind from the 3 km spatial resolution model Nora3 for the region around the CTD stations ($79.9\text{--}80.25^\circ\text{N}$ and $8.5\text{--}11.5^\circ$). The Nora3

model is a Nonhydrostatic High-Resolution Hindcast of the North Sea, the Norwegian Sea, and the Barents Sea (Haakenstad et al., 2021). This model allows for higher spatial resolution north of Svalbard and more accurate wind reanalysis than the ERA5 reanalysis data set (Haakenstad et al., 2021).

Sea ice concentration estimates are from AMSR-2 (Advanced Microwave Scanning Radiometer), derived from brightness temperatures, with a 3.125×3.125 km spatial resolution. They are recovered from the EUMETSAT Ocean and Sea Ice Satellite Application Facility (OSI SAF, www.osi-saf.org). The sea ice edge is defined as the 15% sea ice concentration contour.

3. Results

3.1. From the SeaExplorer Glider

As the glider progresses first northward and then eastward, it encounters diverse water masses with distinct properties in temperature, salinity, chlorophyll a fluorescence, CDOM, and backscatter (Figure 3). The mixed layer depth is defined as the depth where the density increases by 0.03 kg m^{-3} from the surface (Toole et al., 2010).

The western slope of Svalbard (zone 1) hosts the WSC (core with AW reaching $\Theta > 6^\circ\text{C}$ and $S_A > 35.2 \text{ g kg}^{-1}$) as supported by the observed northward depth-averaged current (Figure 1) of about 0.4 m s^{-1} . Two lenses of colder ($\Theta \sim 4^\circ\text{C}$) and fresher ($S_A \sim 35.2 \text{ g kg}^{-1}$) water are observed (Figure 3, the lenses are indicated by an L, and Figure 4g); the first one at the shelf break at about 200 m depth close to bottom; the second one at about 450 m depth already detached from the slope and associated with an offshore shoaling of the isopycnals. The lenses show higher concentrations in CDOM (1.25 ppb compared to 1.1 ppb in the surroundings) and in backscatter ($3.2 \text{ m}^{-1} \text{ sr}^{-1}$ compared to $1.5 \text{ m}^{-1} \text{ sr}^{-1}$ in the surroundings). These lenses originate from the shelf (Koenig et al., 2018; Kolås & Fer, 2018). In this zone, the mixed layer depth varies from 10 m on the shelf to about 50 m in the core of the WSC. Zone 1 hydrographic properties are comparable to those sampled in the WSC in July 2017 (Koenig et al., 2018). The origin of these lenses is discussed in Subsection 4.2.

The three following zones (2 to 4) lie on the YP, where three branches of AW are documented in the literature: the YB following the 1000 m isobath (Cokelet et al., 2008), the YPB that crosses the YP near 700 m depth (Crews et al., 2019; Gascard et al., 1995; Koenig, Provost, Sennechael, et al., 2017; Menze et al., 2019), and the SB that flows along the 400 m isobath.

Zone 2, on the western side of the YP, corresponds to the YB. This branch is slightly colder and fresher than the WSC, especially at the surface where a shallow (~ 5 m) cold and fresh mixed layer is observed (Figure 3). The YB is found on the eastern side of zone 2 with depth-averaged currents $\sim 0.2 \text{ m s}^{-1}$ (Figure 1).

Zone 3 crosses the YPB and is a transition zone between the warm AW and cold Polar Water (Figure 3). A cold and fresh mixed layer is found down to about 40 m depth.

Zone 4 is located on the eastern side of the YP. Temperatures and salinities in the AW are lower than in the previous zones ($\Theta \sim 4^\circ\text{C}$ and $S_A \sim 35 \text{ g kg}^{-1}$ at 100 m), and depth-integrated currents are southward. This water mass may correspond to the return flow of the YB (Athanasé et al., 2021; Meyer et al., 2017). The YB is colder and fresher as these waters have circulated around the YP and mixed with surrounding Polar Waters. The Chlorophyll a fluorescence signal in the fresh and freezing mixed layer is dampened (less than $1 \mu\text{g L}^{-1}$). A near-surface temperature maximum at 20 m depth ($\Theta = 1.5^\circ\text{C}$) is observed (Figure 4 green profiles). The mixed layer is characterized by relatively large CDOM concentration (1.7 ppb), suggesting that the mixed layer is formed from waters that have already partially recirculated in the Arctic Ocean, hence Polar waters (Figure 4g). Indeed, the main source of CDOM in the Arctic is water originating from the Siberian rivers (Athanasé et al., 2019). The large southward flow observed along the eastward slope of the YP ($\sim 0.2 \text{ m s}^{-1}$ in zone 4 mainly, Figure 1b) could be a combination of both the YPB and the return flow of the YB (Athanasé et al., 2021; Meyer et al., 2017).

Zone 5 is located in the Sofia Deep. Zones 4 and 5 are separated by a temperature and salinity front from the surface to at least 700 m depth. The mixed layer is shallow and at the freezing temperature. A strong signal in CDOM (about 1.5 ppb, Figure 3) is observed in the entire water column. At depth, temperature maximum is 2°C and salinity 35.05 g kg^{-1} , characterizing the modified AW (Sundfjord et al., 2020). These waters have been isolated from the surface for a relatively long time (the AOU is the largest reaching $55 \mu\text{mol kg}^{-1}$). They have already recirculated in the Arctic Ocean.

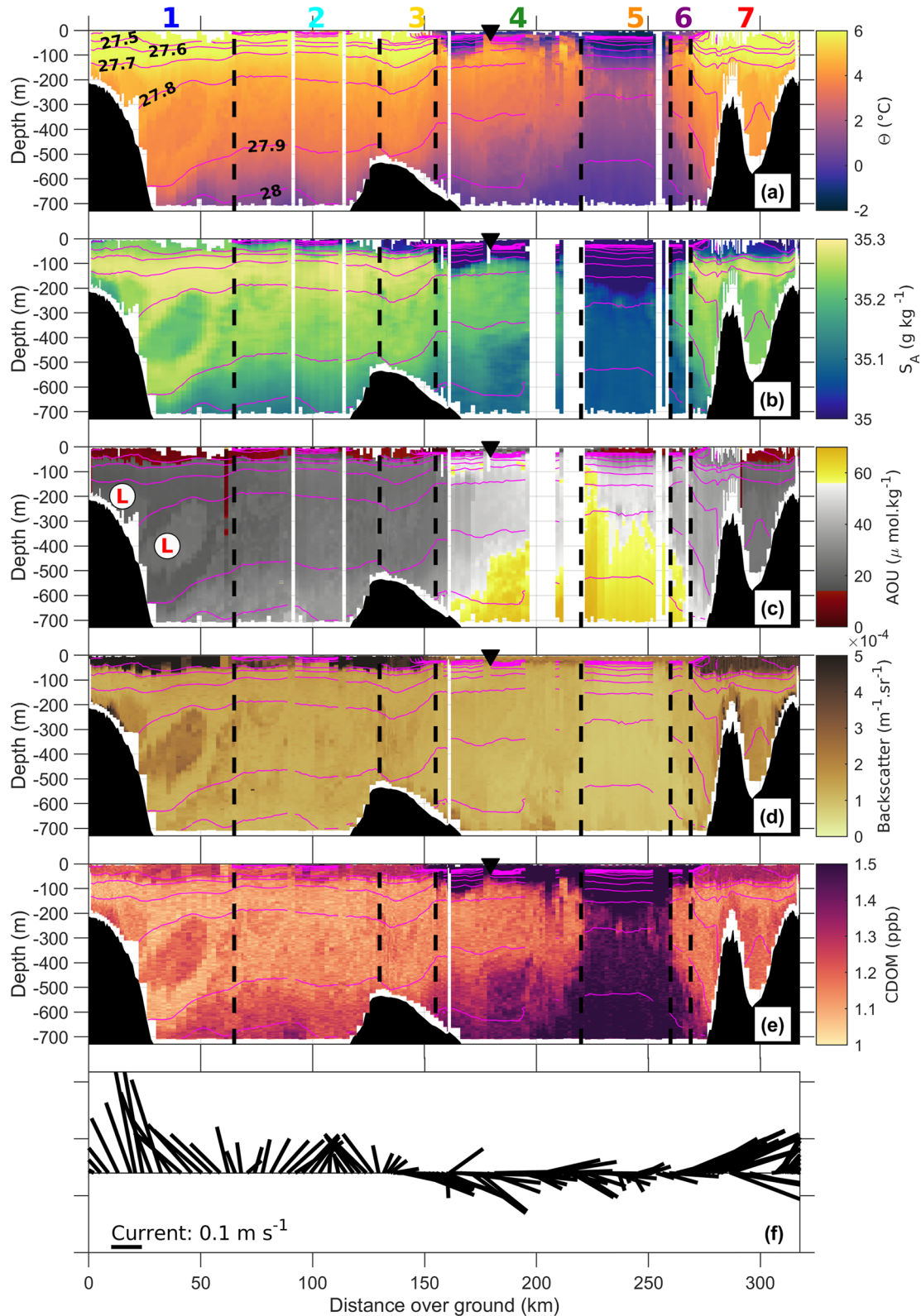


Figure 3. Observations from the glider along the trajectory. (a) Conservative Temperature ($^{\circ}\text{C}$), (b) Absolute Salinity (g kg^{-1}), (c) Apparent Oxygen Utilization ($\mu \text{ mol kg}^{-1}$), (d) total particle concentration ($\text{m}^{-1} \text{sr}^{-1}$), (e) Colored Dissolved Organic Matter (ppb), and (f) depth-integrated current along the glider trajectory. The black-shaded areas are the bathymetry. The dashed vertical lines delineate the different zones that are described in the results section. Pink contours are isopycnals. The 2 circles “L” in panel (c) indicate the location of the cold and fresh lenses discussed in the manuscript.

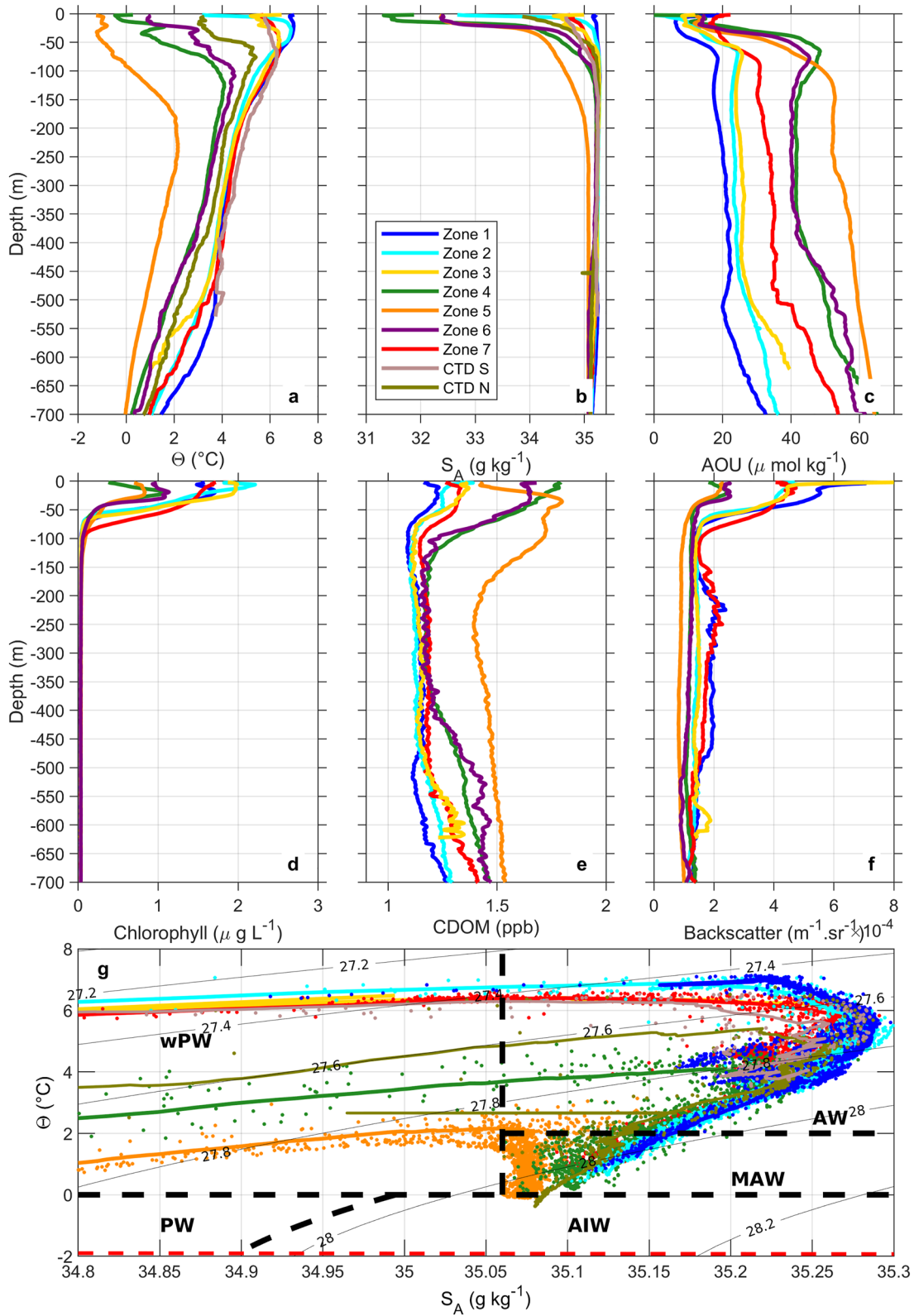


Figure 4.

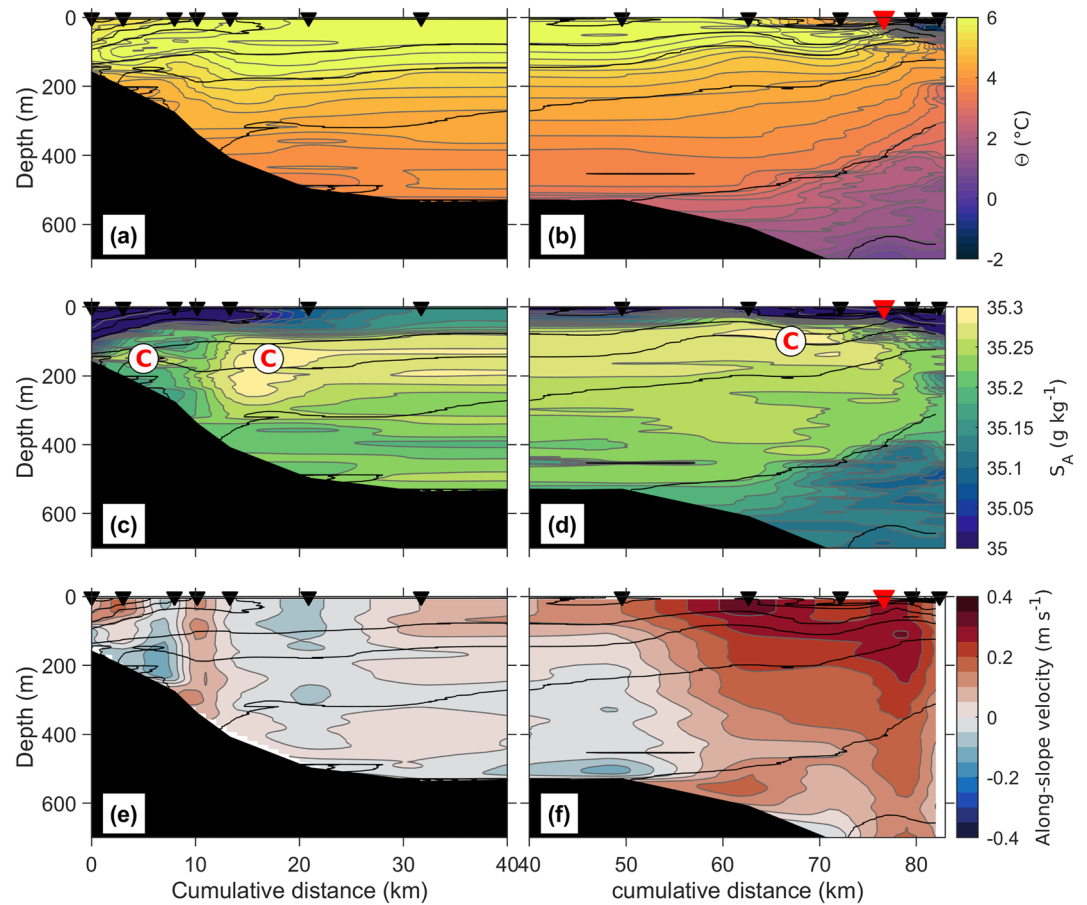


Figure 5. Left panels: southern part of the CTD section across the continental slope (CTD-S in Figure 1). Right panels: northern part of the CTD section across the Yermak Plateau (CTD-N in Figure 1) (a and b) Conservative Temperature ($^{\circ}\text{C}$) (c and d) Absolute Salinity (g kg^{-1}) (e and f) Along-slope velocity (m s^{-1}) deduced from the LADCP data. Data have been interpolated using a spline interpolation with a vertical smoothing of 20 m and a horizontal smoothing of 1 km. Black contours are isopycnals. Black triangles indicate the locations of the CTD stations, and the red one shows the station that is located on the glider track. x axis is the cumulative distance starting from the shallowest station on the slope north of Svalbard. The label “C” in panels (c) and (d) indicates the high salinity cores discussed in the manuscript.

Finally, zone 6 is a transition to zone 7 that sampled the slope north of Svalbard where the SB is located. Depth-averaged currents are large (about 0.4 m s^{-1}), temperature and salinity are similar to the ones in the WSC (zone 1, Figure 4), and mixed layer depth is approximately 40 m.

3.2. From the CTD Section

The southern part of the CTD/LADCP section orientated Southeast–Northwest is shown in Figures 5a, 5c and 5e and the northern part with Southwest–Northeast orientation in Figures 5b, 5d and 5f. The northern part crosses the glider trajectory in zone 4 (black triangles in Figure 3 and red triangle in Figure 5).

At depth above the 200 m isobath, a layer of cold ($\Theta \sim 3^{\circ}\text{C}$) and fresh ($S_A = 35.2 \text{ g kg}^{-1}$) water is observed (Figure 4g, pale pink profile of CTD S). Circulation inshore 400 m isobath is complex. There is no significant eastward velocities above the 400 m isobath as would be expected with the SB (Figure 5e). An eastward flow

Figure 4. Depth-averaged profiles for the different zones delineated in Figure 3 (a) Conservative temperature ($^{\circ}\text{C}$), (b) absolute salinity (g kg^{-1}), (c) apparent oxygen utilization ($\mu\text{mol kg}^{-1}$), (d) chlorophyll a ($\mu\text{g L}^{-1}$), (e) colored dissolved organic matter (ppb), and (f) total particle concentration ($\text{m}^{-1} \text{sr}^{-1}$). (g) Θ - S_A diagram for the different zones with the water masses as defined by Sundfjord et al. (2020). The thick lines are the mean profiles, while the dots are the individual profiles. CTD S: southern part of the CTD section. CTD N: northern part of the CTD section. wPW: winter Polar Water. PW: Polar Water. AIW: Arctic Intermediate Water. MAW: Modified Atlantic Water. AW: Atlantic Water. The red-dotted line is the freezing line.

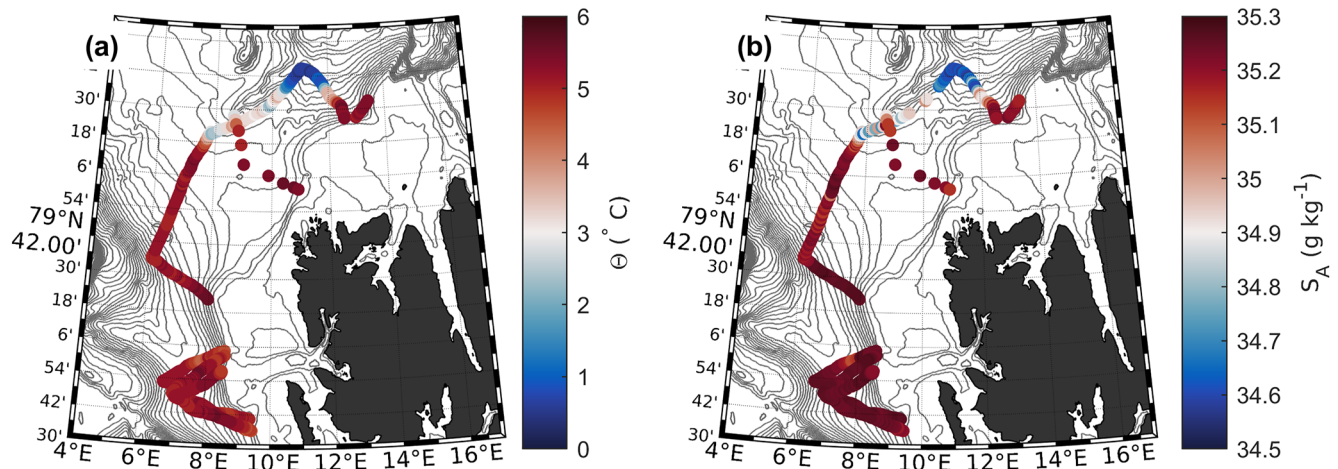


Figure 6. (a) Averaged conservative temperature and (b) averaged absolute salinity in the 0–300 m layer along the glider trajectories and at the CTD stations. Contours are isobaths every 100 m.

is observed above the 300 m isobath with a velocity of about 0.1 ms^{-1} (Figure 5e). Above the 250 m isobath, a reverse westward flow is observed with maximum velocities at 250 m depth $\sim 0.2 \text{ s}^{-1}$. However, all these observations have to be taken with caution as the spatial resolution of the CTD section is relatively coarse (from 2 to 10 km) and some of the patterns described above are only shown at one or two stations (Figure 5).

Several salinity cores (high salinity) are observed in the CTD section. The closest to the shore one is observed at about 180 m depth above the 250 m isobath ($S_A \sim 35.3 \text{ g kg}^{-1}$). This salinity core lies under a layer of fresh water ($S_A < 35 \text{ g kg}^{-1}$) of about 180 m thick at the shallowest station and shoaling to 70 m at km 18 (Figure 5c). A second salinity core is visible at km 17. Finally, the salinity core corresponding to the AW inflow (associated with large along-slope velocity) is observed on the northern section at about 100 m depth above the 700 m isobath associated with large eastward velocities of $\sim 0.4 \text{ m s}^{-1}$ (Figures 5b and 5d and Figures 4a and 4b). It corresponds to the YPB.

3.3. Averaged Temperature and Salinity in the Upper 300 m

Figure 6 showed the averaged temperature and salinity in the upper 300 m. We considered only the profiles deeper than 300 m. For the missing data at the surface, we extrapolated the shallowest measurement if shallower than 10 m. If more data than the upper 10 m were missing, the averaged temperature and salinity in this layer were not computed.

The averaged temperature and salinity in the upper 300 m illustrate the AW mass transformation and pathways over the YP. The western side of the YP is warm and salty as it corresponds to the inflow of the AW through the Fram Strait. Averaged temperature is maximum ($>6^\circ\text{C}$) and averaged salinity is maximum ($>35.3 \text{ g kg}^{-1}$) along the AW inflow, along the WSC and the SB. In contrast, the eastern side of the YP is fresher and colder, an indication of the transformation of the AW above and around the YP. In the YB (zone 4), the averaged salinity is about 34.9 g kg^{-1} and the averaged temperature about 3°C . The lowest temperature average (0°C) and salinity average (34.5 g kg^{-1}) are found in the Sofia Deep where there is no AW.

At the intersection of the CTD section with the glider trajectory on the YP (at 9°E , 80.4°N), glider data exhibit lower salinity and lower temperature than the CTD section. The glider was first to sample this location on 19 September 2017, while the CTD station was done a few days later on 24 September 2017. During these five days, both the sea ice edge (Figure 1) and the associated low surface salinity caused by melting sea ice moved northward. The temperature and salinity averages below 50 m (50–300 m) at the two dates are comparable (glider trajectory and CTD section, not shown). Thus, the differences in surface temperature and salinity averages at this intersection are caused by the northward advection of the sea ice and the surface fresh layer of meltwater over a few days due to wind forcing.

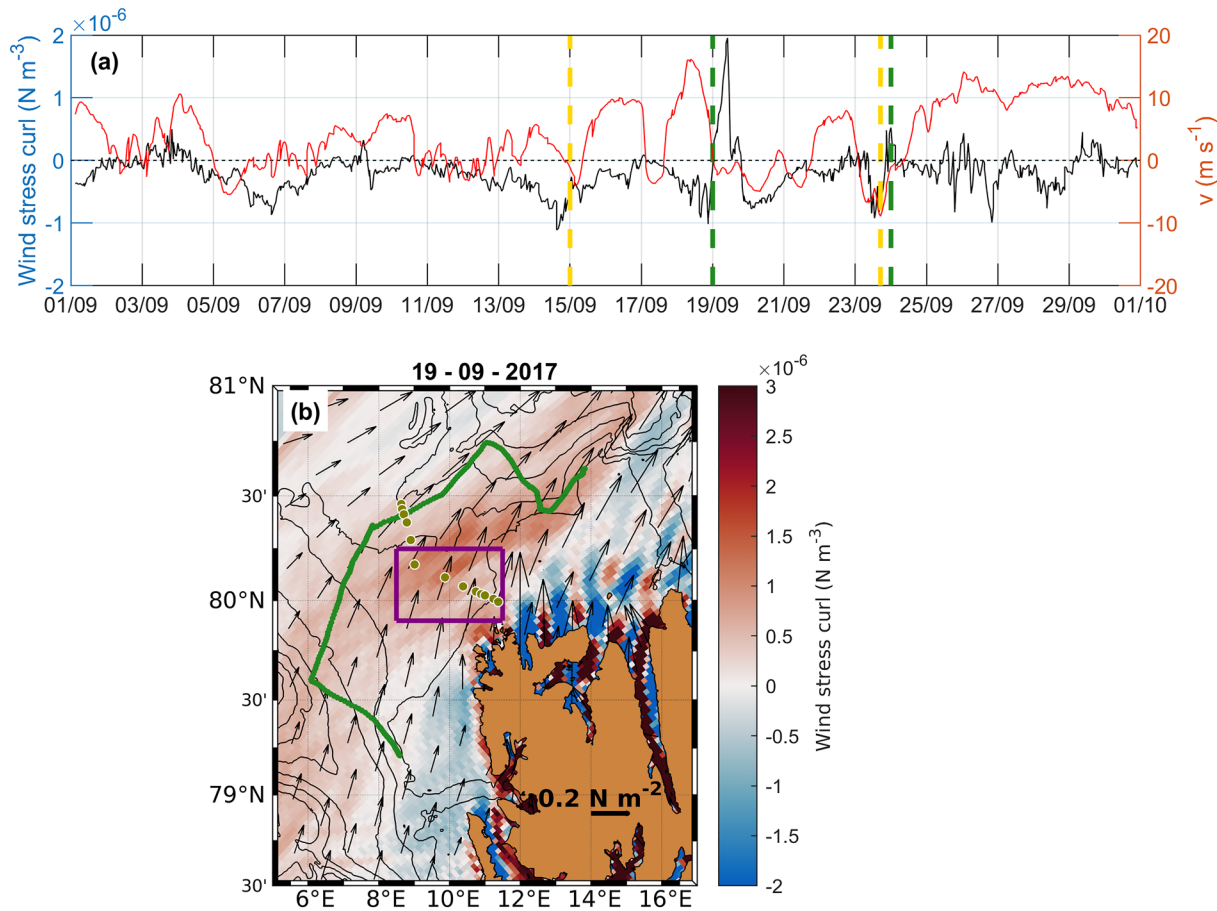


Figure 7. (a) Time series of left axis: wind stress curl (in N m^{-3}) and right axis: meridional wind velocities (in m s^{-1}) from the model Nora3 averaged over the purple box in (b). The green-dashed lines indicate 19 (date of Figures 7b) and 24 September 2017 (date of the CTD transect). The yellow-dashed lines indicate the glider mission. (b) Map of wind stress curl on 19 September 2017. Arrows are the wind stress from Nora3 (in N m^{-2}), plotted every 8 data points. Black contours are bathymetry contours every 400 m. The green line is the glider trajectory and the green dots indicate the locations of the CTD stations.

4. Discussion

4.1. Anomalous Wind Forcing in Summer 2017

Winds in summer 2017 were anomalously blowing from the south as shown in Figure 2. Wind stress curl estimated from the high-resolution model (Nora3) in the area of the CTD section was strongly positive during 19–20 September (Figure 7a). This positive wind stress curl is associated with southerly wind rotating toward southwesterlies (Figure 7b). These strong southerly winds can explain some specific patterns documented by both the glider and the ship-based observations as explained in the following subsections.

4.2. Formation Mechanism of the Cold and Fresh Water Lenses

Lenses of cold and fresh waters were sampled in July 2017 in the WSC (Koenig et al., 2018) and in September 2017 (two lenses in Figure 3 indicated with an L). These lenses were observed at different stages: from just formed cold, fresh, CDOM-enriched, and oxygen-depleted water lenses at the bottom on the shelf break to detached lenses in the AW inflow. Once offshore (in the WSC), the lenses we observed stabilized at their density level at about 300 m depth (Figure 3), which is below the core of the AW (around 150 m depth, Figure 3). Hence, the lenses described here cool and freshen the AW core from below.

The detachment of the cold and fresh lenses from the shelf in the WSC can be a consequence of the southerly wind bursts and their subsequent relaxation (Figures 2 and 7a) (Koenig et al., 2018). As suggested by Nilsen et al. (2016), southerly winds set up a surface onshore Ekman transport of warm and salty water inducing mixing

on the shelf. Once the southerly wind event relaxes, denser cold and fresh water lenses at depth on the shelf can detach and be found in the core of the boundary current.

Kolås and Fer (2018) documented similar lenses in the WSC. They suggest that the lenses originate from convectively driven bottom mixing followed by the detachment of the mixed fluid and its transfer into the ocean interior. Indeed, a mean current flowing along the slope in the direction of Kelvin wave propagation can induce a downslope Ekman transport that advects lighter waters under denser waters, driving diapycnal mixing (Kolås & Fer, 2018).

The two processes described above do not exclude each other.

4.3. Impact of Winds on the Svalbard Branch

In September 2017, the SB was not well constrained at the 400–500 m isobath that it usually follows, and a bottom-intensified westward current was observed inshore at the 250 m isobath.

The bottom intensified westward velocities above the 300 m isobath were associated with an eastward flow at the 300 m isobath at the shelf break (Figure 5e, km 7). We could speculate that it was the signature of an eddy with a radius of about 4 km, which corresponds to the Rossby radius of deformation in the area (Zhao et al., 2014). In the region, eddies are relatively common (Crews et al., 2018). However, the spatial resolution of the CTD data prevents us from confirming the presence of an eddy.

We believe that one of the main factors influencing the ocean dynamics in the region is the anomalous wind pattern in September 2017. The CTD section was performed on 24 September, 4 days after a large southerly wind event during 18–20 September and during a small positive wind stress curl event on 24 September (Figure 7). The wind stress curl event intensity on 19–20 reaches 2×10^{-6} , which is of similar order of magnitude as the wind events discussed in Nilsen et al. (2021). As suggested by Nilsen et al. (2021), the variability in the SB is controlled by the wind stress curl on the shelf. The geostrophic adjustment is short about 12–15hr according to Nilsen et al. (2021). Over the 18–20 September period, the wind stress curl above the continental slope was positive (Figure 7a), leading to a decrease in the strength of the SB, due to a divergence of surface waters and a decrease in the sea surface tilt toward the coast. Although this wind event occurs 4 days before the CTD section was performed, its signature on the ocean density structure and current flows may remain several days. The strongly anomalous southerly wind conditions and associated adjustments of ocean isopycnals can explain why the SB was weak at its usual 400 m isobath location on 24 September in our observations.

5. Conclusion

We described the AW circulation and properties north of Svalbard in September 2017 combining ocean glider data and hydrographic observations. Part of the AW pathway over the YP was anomalous and several cold fresh-water lenses were observed detaching from the Svalbard Shelf. The sampling was performed after a period of southerly winds, an unusual situation for the region and the season. Over the 2010–2020 period, most of the southerly wind events occurred in winter and were associated with polar lows (Woods & Caballero, 2016). Strong southerly winds with a meridional component larger than 8 m s^{-1} represent less than 5% in that 2010–2020 period. However, the year 2017 was peculiar with southerly winds twice more frequent than during the reference 2010–2020 period.

Concurrent to these southerly wind conditions, we observed widespread cold freshwater lenses north and west of Svalbard that had detached from the shelf. Being cold and fresh, the lenses contribute to the cooling and freshening of the warmer AW inflow as they detach into it and mix. Further investigation is needed to quantify the importance of the lenses in the transformation of the AW along the Arctic inflow pathway. The region north and west of Svalbard is a hotspot for shelf-slope exchanges (Luneva et al., 2020).

In September 2017, the current associated with the SB on the YP was not at its usual location at the 400–500 m isobath. The large variability of the SB current intensity has been documented in Koenig, Provost, Sennechael, et al. (2017) and Athanase et al. (2021) using high-resolution operational model outputs, and has shown a particularly weak SB at the shelf break in September 2017. Here, we propose that the strong and anomalous southerly wind conditions and the strong positive wind stress curl event in September 2017 led to a divergence of the

surface waters and a geostrophic adjustment, resulting in a weaker flow in the SB. Southerly wind conditions are increasing in the Arctic as the number of cyclones influencing Svalbard has increased during winter over the past 4 decades (Wickström et al., 2020). We can hence expect that the ocean circulation documented in September 2017 could become more frequent in the future.

In the context of climate change, understanding the dynamics and the changes in the inflow of warm saline AWs into the Arctic Ocean through the Nordic Seas is of great importance with impacts on Arctic water stratification, eddy fluxes, heat fluxes across the ocean-sea ice-atmosphere interfaces, and vertical mixing among other things. Monitoring the rapid changes in the AW inflow pathways and impacts further into the Arctic Ocean should stay at the forefront of the Arctic oceanography. As such, gliders are a useful oceanographic tool to investigate small-scale processes in polar regions and near sea ice.

Data Availability Statement

The glider data are publicly available in the SEANOE database: <https://doi.org/10.17882/81755>.

Acknowledgments

The glider work was supported by the European project ACCESS (Number: 265863). We thank Norwegian Polar Institute and the captain and crew onboard the R/V Lance for the logistics of the glider deployment and recovery. We also thank all the glider pilots from Alseamar. Z. Koenig acknowledges post-doctoral research fellow funding from the Pan-Arctic Option Belmont Forum and from the Nansen Legacy Project (Norwegian research council project number 276730). A. Meyer was supported by the Australian Research Council Centre of Excellence for Climate Extremes (CE170100023), the Australian Research Council Discovery Early Career Research Award project DE200100414, and the Norwegian Polar Institute's Centre for Ice, Climate and Ecosystems. A. Sundfjord acknowledges the Fram Centre Arctic Ocean project A-TWAIN for funding.

References

- Årthun, M., Eldevik, T., Smedsrud, L., Skagseth, Ø., & Ingvaldsen, R. (2012). Quantifying the influence of Atlantic heat on Barents Sea ice variability and retreat. *Journal of Climate*, 25(13), 4736–4743. <https://doi.org/10.1175/JCLI-D-11-00466.1>
- Asbjørnsen, H., Årthun, M., Skagseth, Ø., & Eldevik, T. (2020). Mechanisms underlying recent Arctic atlantification. *Geophysical Research Letters*, 47(15), e2020GL088036. <https://doi.org/10.1029/2020GL088036>
- Athanase, M., Provost, C., Artana, C., Pérez-Hernández, M. D., Sennéchaël, N., Bertosio, C., et al. (2021). Changes in Atlantic Water circulation patterns and volume transports North of Svalbard over the last 12 years (2008–2020). *Journal of Geophysical Research: Oceans*, 126(1), e2020JC016825. <https://doi.org/10.1029/2020JC016825>
- Athanase, M., Provost, C., Pérez-Hernández, M. D., Sennéchaël, N., Bertosio, C., Artana, C., et al. (2020). Atlantic Water modification north of Svalbard in the Mercator physical system from 2007 to 2020. *Journal of Geophysical Research: Oceans*, 125(10), e2020JC016463. <https://doi.org/10.1029/2020jc016463>
- Athanase, M., Sennéchaël, N., Garric, G., Koenig, Z., Boles, E., & Provost, C. (2019). New hydrographic measurements of the upper arctic Western Eurasian Basin in 2017 reveal fresher mixed layer and shallower warm layer than 2005–2012 climatology. *Journal of Geophysical Research: Oceans*, 124(2), 1091–1114. <https://doi.org/10.1029/2018JC014701>
- Cokelet, E. D., Tervalon, N., & Bellingham, J. G. (2008). Hydrography of the West Spitsbergen current, svalbard branch: Autumn 2001. *Journal of Geophysical Research*, 113(C1), C01006. <https://doi.org/10.1029/2007JC004150>
- Crews, L., Sundfjord, A., Albreten, J., & Hattermann, T. (2018). Mesoscale eddy activity and transport in the Atlantic water inflow North of Svalbard. *Journal of Geophysical Research: Oceans*, 123(1), 201–215. <https://doi.org/10.1002/2017JC013198>
- Crews, L., Sundfjord, A., & Hattermann, T. (2019). How the yermak pass branch regulates Atlantic water inflow to the Arctic Ocean. *Journal of Geophysical Research: Oceans*, 124(1), 267–280. <https://doi.org/10.1029/2018JC014476>
- Erofeeva, S., & Egbert, G. (2020). Arc5km2018: Arctic ocean inverse tide model on a 5 kilometer grid, 2018. *Arctic Data Center*, 10, A21R6N14K. <https://doi.org/10.18739/A21R6N14K>
- Garau, B., Ruiz, S., Zhang, W. G., Pascual, A., Heslop, E., Kerfoot, J., & Tintoré, J. (2011). Thermal lag correction on slocum CTD glider data. *Journal of Atmospheric and Oceanic Technology*, 28(9), 1065–1071. <https://doi.org/10.1175/jtech-d-10-05030.1>
- Gascard, J.-C., Richez, C., & Rouault, C. (1995). New insights on large-scale oceanography in Fram Strait: The West Spitsbergen current. *Coastal and Estuarine Studies*, 131. <https://doi.org/10.1029/ce049p0131>
- Haakenstad, H., Breivik, Ø., Furevik, B. R., Reistad, M., Bohlinger, P., & Aarnes, O. J. (2021). Nora3: A nonhydrostatic high-resolution hindcast of the North sea, the Norwegian sea, and the Barents sea. *Journal of Applied Meteorology and Climatology*, 60(10), 1443–1464. <https://doi.org/10.1175/JAMC-D-21-0029.1>
- Hattermann, T., Isachsen, P. E., von Appen, W.-J., Albreten, J., & Sundfjord, A. (2016). Eddy-driven recirculation of Atlantic water in Fram Strait. *Geophysical Research Letters*, 43(7), 3406–3414. <https://doi.org/10.1002/2016GL068323>
- Hersbach, H., Bell, B., Berrisford, P., Biavati, G., Horányi, A., Muñoz Sabater, J., et al. (2018). Era5 hourly data on single levels from 1979 to present. *Copernicus Climate Change Service (C3S) Climate Data Store (CDS)*, 10. <https://doi.org/10.24381/cds.adbb2d47>
- Ivanov, V., Alexeev, V., Koldunov, N. V., Repina, I., Sandø, A. B., Smedsrud, L. H., & Smirnov, A. (2016). Arctic Ocean heat impact on regional ice decay: A suggested positive feedback. *Journal of Physical Oceanography*, 46(5), 1437–1456. <https://doi.org/10.1175/JPO-D-15-0144.1>
- Jakobsson, M., Mayer, L., Coakley, B., Dowdeswell, J. A., Forbes, S., Fridman, B., et al. (2012). The international bathymetric chart of the Arctic Ocean (IBCAO) version 3.0. *Geophysical Research Letters*, 39(12). <https://doi.org/10.1029/2012gl052219>
- Koenig, Z., Beguery, L., Provost, C., Meyer, A., Sundfjord, A., Athanase, M., & Gascard, J.-C. (2017). SeaExplorer glider SEA028 observations West of Svalbard in [Dataset]. Seanoe Database. <https://doi.org/10.17882/56366>
- Koenig, Z., Beguery, L., Provost, C., Meyer, A., Sundfjord, A., & Gascard, J.-C. (2017). SeaExplorer glider SEA028 observations North of Svalbard in September 2017 [Dataset]. Seanoe Database. <https://doi.org/10.17882/81755>
- Koenig, Z., Meyer, A., Provost, C., Sennéchaël, N., Sundfjord, A., Beguery, L., et al. (2018). Cooling and freshening of the West Spitsbergen current by shelf-origin cold core lenses. *Journal of Geophysical Research: Oceans*, 123(11), 8299–8312. <https://doi.org/10.1029/2018JC014463>
- Koenig, Z., Provost, C., Sennéchaël, N., Garric, G., & Gascard, J.-C. (2017). The Yermak Pass Branch: A major pathway for the Atlantic water North of Svalbard? *Journal of Geophysical Research: Oceans*, 122(12), 9332–9349. <https://doi.org/10.1002/2017JC013271>
- Koenig, Z., Provost, C., Villaceros-Robineau, N., Sennéchaël, N., Meyer, A., Lellouche, J.-M., & Garric, G. (2017). Atlantic waters inflow North of Svalbard: Insights from IAOOS observations and Mercator ocean global operational system during N-ICE2015. *Journal of Geophysical Research: Oceans*, 122(2), 1254–1273. <https://doi.org/10.1002/2016JC012424>
- Kolås, E., & Fer, I. (2018). Hydrography, transport and mixing of the West Spitsbergen current: The Svalbard branch in summer 2015. *Ocean Science*, 14(6), 1603–1618. <https://doi.org/10.5194/os-14-1603-2018>

- Luneva, M. V., Ivanov, V. V., Tuzov, F., Aksenov, Y., Harle, J. D., Kelly, S., & Holt, J. T. (2020). Hotspots of dense water cascading in the Arctic ocean: Implications for the Pacific water pathways. *Journal of Geophysical Research: Oceans*, *125*(10), e2020JC016044. <https://doi.org/10.1029/2020JC016044>
- McDougall, J., & Barker, P. (2011). Getting started with TEOS-10 and the gibbs seawater (GSW) oceanographic toolbox, 28pp. SCOR/IAPSO WG127 (ISBN: 978-0-646-55621-5).
- Menze, S., Ingvaldsen, R. B., Haugan, P., Fer, I., Sundfjord, A., Beszczynska-Moeller, A., & Falk-Petersen, S. (2019). Atlantic water pathways along The north-Western Svalbard shelf mapped using vessel-mounted current profilers. *Journal of Geophysical Research: Oceans*, *124*(3), 1699–1716. <https://doi.org/10.1029/2018JC014299>
- Meyer, A., Sundfjord, A., Fer, I., Provost, C., Villacieros Robineau, N., Koenig, Z., et al. (2017). Winter to summer oceanographic observations in the Arctic Ocean north of Svalbard. *Journal of Geophysical Research: Oceans*, *122*(8), 6218–6237. <https://doi.org/10.1002/2016JC012391>
- Nilsen, F., Ersdal, E. A., & Skogseth, R. (2021). Wind-driven variability in the Spitsbergen polar current and the Svalbard branch across the Yermak plateau. *Journal of Geophysical Research: Oceans*, *126*(9). <https://doi.org/10.1029/2020JC016734>
- Nilsen, F., Skogseth, R., Vaardal-Lunde, J., & Inall, M. (2016). A simple shelf circulation model: Intrusion of Atlantic water on the West Spitsbergen shelf. *Journal of Physical Oceanography*, *46*(4), 1209–1230. <https://doi.org/10.1175/jpo-d-15-0058.1>
- Polyakov, I. V., Pnyushkov, A. V., Alkire, M. B., Ashik, I. M., Baumann, T. M., Carmack, E. C., et al. (2017). Greater role for Atlantic inflows on sea-ice loss in the Eurasian Basin of the Arctic Ocean. *Science*, *356*(6335), 285–291. <https://doi.org/10.1126/science.aai8204>
- Skagseth, Ø., Eldevik, T., Årthun, M., Asbjørnsen, H., Lien, V. S., & Smedsrud, L. H. (2020). Reduced efficiency of the Barents sea cooling machine. *Nature Climate Change*, *10*(7), 661–666. <https://doi.org/10.1038/s41558-020-0772-6>
- Sundfjord, A., Assmann, K. M., Lundesgaard, Ø., Renner, A. H., Lind, S., & Ingvaldsen, R. B. (2020). Suggested water mass definitions for the central and northern Barents sea, and the adjacent Nansen basin. *The Nansen Legacy Report Series*(8). <https://doi.org/10.7557/nlrs.5707>
- Thurnherr, A. (2011). How to process LADCP data with the LDEO software. version IX.5.
- Toole, J. M., Timmermans, M.-L., Perovich, D. K., Krishfield, R. A., Proshutinsky, A., & Richter-Menge, J. A. (2010). Influences of the ocean surface mixed layer and thermohaline stratification on Arctic Sea ice in the central Canada Basin. *Journal of Geophysical Research*, *115*(C10), 2009JC005660. <https://doi.org/10.1029/2009jc005660>
- Tsubouchi, T., Bacon, S., Aksenov, Y., Naveira Garabato, A. C., Beszczynska-Möller, A., Hansen, E., et al. (2018). The Arctic Ocean seasonal cycles of heat and freshwater fluxes: Observation-based inverse estimates. *Journal of Physical Oceanography*, *48*(9), 2029–2055. <https://doi.org/10.1175/JPO-D-17-0239.1>
- von Appen, W.-J., Schauer, U., Hattermann, T., & Beszczynska-Möller, A. (2016). Seasonal cycle of mesoscale instability of the West Spitsbergen current. *Journal of Physical Oceanography*, *46*(4), 1231–1254. <https://doi.org/10.1175/jpo-d-15-0184.1>
- Wickström, S., Jonassen, M. O., Vihma, T., & Uotila, P. (2020). Trends in cyclones in the high-latitude north atlantic during 1979–2016. *Quarterly Journal of the Royal Meteorological Society*, *146*(727), 762–779. <https://doi.org/10.1002/qj.3707>
- Woods, C., & Caballero, R. (2016). The role of moist intrusions in winter arctic warming and sea ice decline. *Journal of Climate*, *29*(12), 4473–4485. <https://doi.org/10.1175/jcli-d-15-0773.1>
- Zhao, M., Timmermans, M.-L., Cole, S., Krishfield, R., Proshutinsky, A., & Toole, J. (2014). Characterizing the eddy field in the Arctic Ocean halocline. *Journal of Geophysical Research*, *119*(12), 8800–8817. <https://doi.org/10.1002/2014jc010488>